Modelling motion instabilities of a submerged wave energy converter

Dirk Rijnsdorp[1,†],Jana Orszaghova[1], David Skene[1], Hugh Wolgamot[1],Ashkan Rafiee[2]

[1]The University of Western Australia, WA 6009, Australia, [†]dirk.rijnsdorp@uwa.edu.au

[2]Carnegie Clean Energy Ltd, Belmont, Australia

Introduction

Floating structures can be prone to dynamic instabilities (also known as parametric excitations) that can result in large motions even in the absence of direct external excitation, like that from waves, in the unstable mode (e.g., Paulling and Rosenberg, 1959; Koo and Kim, 2004; Babarit et al., 2009; Orszaghova et al., 2018b). In general, such motion instabilities are undesirable as they can degrade design life and operational performance of offshore structures.

Theoretical investigations of instabilities rely on analysis of the well-known Mathieu equation. Resulting stability diagrams (also known as Ince-Strutt diagrams) reveal bounded and unbounded solution regions depending on the amplitude and frequency of the parametric excitation (see Fig. 1b). Although such theoretical analysis may reveal the presence of instability, it cannot provide information on the severity of the unstable motions. CFD models provide the most advanced numerical technique to study the presence and magnitude of such instabilities as they can account for the relevant physical processes, including viscous effects. However, due to their vast computational requirements, the application of such models is limited, and they are only suitable to run a select number of simplified sea states (e.g., monochromatic waves or design wave groups).

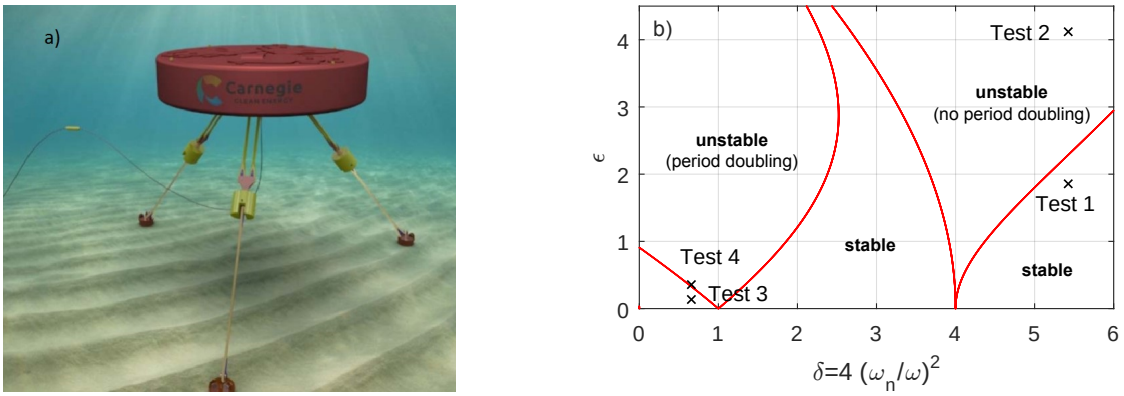

Figure 1: Panel a: Diagram of the muti-moored CETO wave energy converter. Panel b: Stability diagram and test conditions considered in this work.

In this paper, we attempt to predict the motion instabilities of a wave energy converter using (a) the widely known and used Cummins' equation model (Cummins, 1962), which couples linear hydrodynamics to nonlinear mooring/power take-off forces, and (b) a non-hydrostatic wave-flow model called SWASH (Simulating WAves till SHore). The SWASH model (Zijlema et al., 2011) provides an efficient direct numerical implementation of the basic flow equations (akin to CFD). The model has recently been extended to include dynamic coupling to the rigid body equations to account for the interactions between waves and floating bodies (Rijnsdorp et al., 2018). When compared to conventional CFD codes, the primary advantage of the non-hydrostatic models like SWASH is that they can resolve the nonlinear wave dynamics and wave-structure interactions with a significantly coarser grid resolution. As such, they allow for applications at the scale of a field site, as well as for longer simulation durations that are essential to elucidate motion instabilities for realistic sea states. In this work, we present an initial effort to compare predictions by the SWASH model with the Cummins' equation and observations from an experimental campaign on yaw instability in the multi-moored CETO wave energy converter developed by Carnegie Clean Energy (Fig. 1a).

Experimental set-up

As part of an ongoing collaboration between Carnegie Clean Energy and the University of Western Australia, motion instabilities of the CETO wave energy converter were investigated in the Ocean Wave Basin at the University of Plymouth, UK. The CETO device is an axi-symmetric submerged

buoy (a truncated vertical cylinder), which is taut-moored (symmetrically) via three inclined tethers (Fig. 1a). The mooring and the power take-off (PTO) systems are integrated, and power is absorbed from the dynamic extensions and retractions of the tethers. Although hydrodynamic excitation in yaw is absent for such a cylindrical axi-symmetric device, yaw instability may develop due to nonlinear coupling between yaw and heave (in the PTO-mooring system).

Fig. 1b shows the Ince-Strutt stability diagram of the CETO device as given by the Mathieu equation. In it, the horizontal axis δ is related to the ratio of the natural yaw frequency (ω_n) and the frequency of the parametric excitation (ω); and the vertical axis ϵ is related to the magnitude of the parametric excitation. Note that in the CETO system studied here, ϵ depends on the heave motion amplitude as well as the PTO-mooring parameters (refer to Orszaghova et al., 2018a, for more details). During the experimental campaign, various wave conditions were explored that spanned both the stable and unstable regions in this stability diagram. In this work, we consider two pairs of regular wave experiments. Each pair includes two tests with the same wave period T but different wave heights H, thereby including both stable (for the smaller H) and unstable (for the larger H) yaw motions.

Numerical methodology

The non-hydrostatic model SWASH (Zijlema et al., 2011) is a direct numerical implementation of the three-dimensional Euler or Reynolds Averaged Navier Stokes (RANS) equations (when viscous stresses are included) on a curvilinear terrain-following grid. In contrast to conventional CFD models, which aspire to resolve complex details of the free surface (for example, using the level-set or VOF method), non-hydrostatic models rely on the significant simplifying assumption that the free-surface can be represented by a single valued function. This simplification, combined with the use of efficient numerical schemes (e.g., Stelling and Zijlema, 2003), allows non-hydrostatic models to efficiently capture nonlinear wave and flow dynamics at the scale of a realistic coastal region.

Recently, efforts have been made to extend this modelling approach to account for interactions between waves and floating bodies (e.g., Rijnsdorp and Zijlema, 2016; Ma et al., 2016). In particular, Rijnsdorp et al. (2018) extended the SWASH model to capture wave-induced response of a submerged wave-energy converter. An iterative approach was implemented to account for the dynamic coupling between the flow and the motions of the floating body (accounting for the full geometric nonlinearity of the mooring system), see Fig. 2 for a sketch of the grid schematization and the governing equations. To preserve the efficiency of the numerical approach, the kinematic boundary conditions (kbc) were

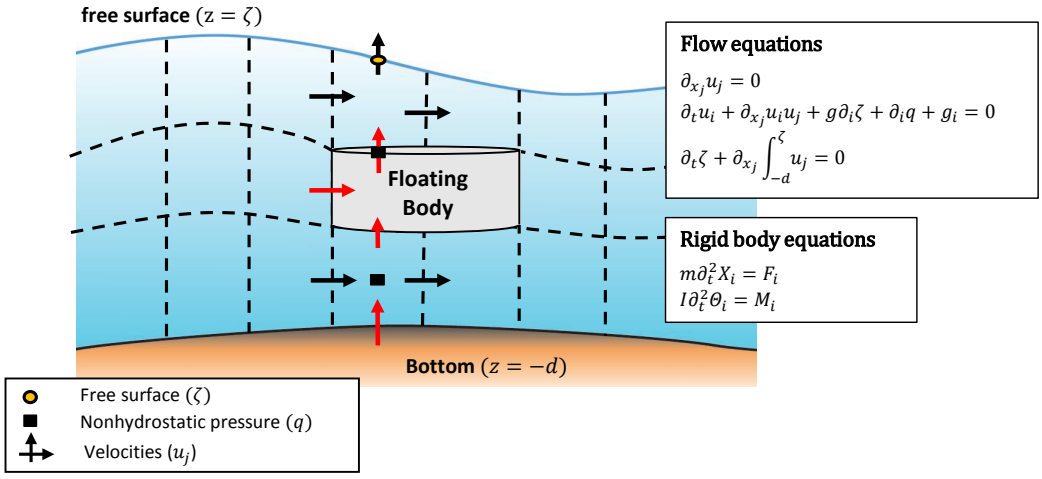

Figure 2: Sketch of the terrain-following grid schematization, the staggered variable arrangement, and the governing equations for the flow and the body motions. In the flow equations, t is time, x_i are the Cartesian coordinates, u_i are the velocity components, g_i ($= \langle 0, 0, g \rangle$) is the gravitational acceleration, and q is the non-hydrostatic pressure. In the rigid body equations, m and I are the mass and moment of inertia matrices, X_i and Θ_i represent the body translations and rotations, and F_i and M_i represent the external forces acting on the body (including the hydrodynamic and mooring line forces). The color of the arrows indicate whether the velocity is computed using the momentum equation (black arrow), or imposed through the kinematic boundary condition.

linearized for the surge and sway motions (by not adapting the flow grid for these body motions), whereas the fully nonlinear kbc were used for the remaining body motions (see Rijnsdorp et al., 2018, for more details). This implies that the model captures the partially nonlinear hydrodynamics in surge and sway and the fully nonlinear hydrodynamics of the remaining degrees of freedom.

Although viscous effects can in principle be captured, a fine spatial and temporal resolution is required to accurately resolve these effects. However, in accordance with the philosophy of the non-hydrostatic approach, we adopt a relatively coarse resolution and therefore neglect the viscous stresses in the computation (i.e., solving the Euler equations), and note that viscous damping of the body motions is not accounted for.

All simulations were carried out using a rectilinear grid with five terrain following layers in the vertical and with a horizontal spatial resolution that ensured at least 20 points per wave length and 10 points per cylinder diameter. This resulted in a total of 33,925–84,390 cells across the different simulations. The time step was dynamically updated during the simulation to ensure that the Courant stability criterion was satisfied. Simulations of 4 min real time took about 45min to complete on a local desktop using 6 cores. The buoy motions in the simulations were initialized with a small yaw (1°) to reduce the time required for the yaw instabilities to develop.

Results

Fig. 3 shows the predicted and measured time series of the heave and yaw motions for the four test cases considered. For the first pair of test conditions (Test 1 and 2, with the same incident wave period $T = 2.6$ s), the yaw motion remained small for $H = 0.1$ m (Fig. 3a-b), whereas yaw instabilities developed for a wave height of $H = 0.2$ m (Fig. 3c-d). The period of the unstable yaw motion equalled that of the heave motion and thus the wave excitation. For both test conditions, the two models captured the overall response of the device, and the yaw instability that developed during Test 2. Both models also captured the typical magnitude and nonlinear shape of both the heave and yaw oscillation, and the negative mean drift in heave for Test 2 which occurred as the yaw instability developed.

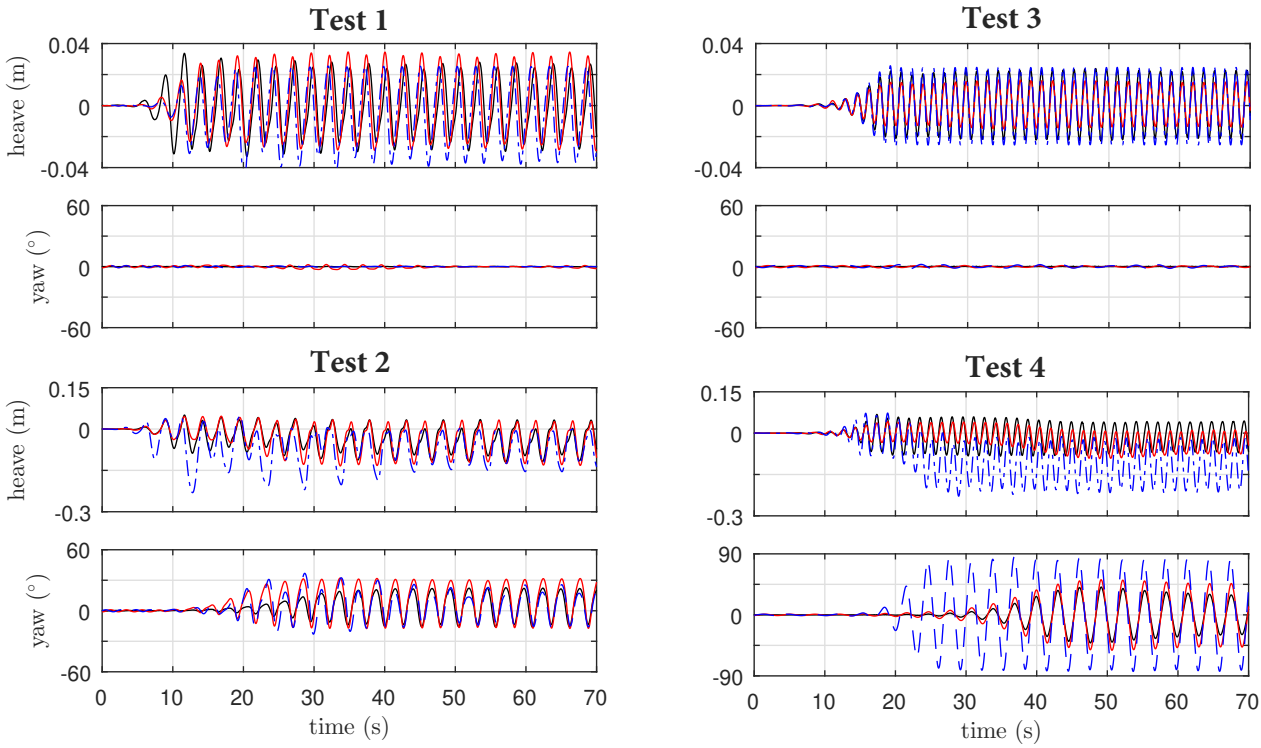

Figure 3: Time series of the measured (black line), and predicted (Cummins' equation, dash dotted blue line; SWASH, full red line) heave and yaw motion for the four test cases. Test 1 and 2 considered monochromatic waves with period $T = 2.6$ s and wave heights $H = 0.1$ and 0.2 m, respectively. Test 3 and 4 considered monochromatic waves with period $T = 1.53$ s and wave heights $H = 0.1$ and 0.3 m, respectively.

Similarly, both models captured the occurrence of the yaw instability in the second pair of experimental observations (Fig. 3e-h). Importantly, they also captured the period doubling of the yaw response for Test 4, which is characteristic for the first instability branch (see Figure 1b). Differences between both models and the observations were largest for this test case. Both the magnitude of the yaw instability and the heave motions (including the mean drift) were greatly over predicted by the time-domain model based on the Cummins' equations. The SWASH predictions were generally in better agreement with the observations, although it also over predicted the magnitude of the yaw instability and the mean drift in heave. The improved accuracy of the SWASH predictions compared to the Cummins' equations is potentially related to its inclusion of nonlinear excitation forces and the nonlinear hydrodynamics for some of the modes (i.e., heave, pitch and roll).

Overall, the SWASH model captured the response of the body with pleasing accuracy, especially given the coarse resolutions that were used in this work. Nonetheless, the magnitude of the yaw motion is typically over-predicted by the model for both unstable cases. This is likely due to the omission of viscous stresses, and thereby the absence of viscous damping on the yaw motion.

As an alternative to running the SWASH simulations with high resolutions to capture the viscous stresses, we aim to parametrise the viscous damping of the various modes as part of future work. At the workshop, we will present results of both regular and irregular test cases including the parametrisation of viscous damping. With this parametrisation we expect the SWASH model to better capture the maximum amplitude of the instability. As such, we believe that the resulting model can provide insight on the influence of instabilities on power capture under realistic sea states, and that it can be used to explore design changes aimed at minimizing the undesired instabilities.

Acknowledgements

This research was supported by the Australian Renewable Energy Agency (ARENA) as part of ARENA's Research and Development Program in a joint project with Carnegie Clean Energy (grant number 2015RND086), and the Australian Research Council's Linkage Project scheme (LP150100598). The laboratory tests performed at the COAST lab Ocean basin at the University of Plymouth, UK were supported by MaRINET2 funding (Project ID 1299). Provision of the experimental data from Carnegie Clean Energy is gratefully acknowledged. Parts of this research were conducted by the Wave Energy Research Centre and partly funded by the Department of Primary Industries and Regional Development (DPIRD).

References

Babarit, A., Mouslim, H., Clément, A., Laporte-Weywada, P., 2009. On the numerical modelling of the nonlinear behaviour of a wave energy converter, in: International Conference on Offshore Mechanics and Arctic Engineering, ASME, Honolulu, Hawai, 1045–1053.

Cummins, W.E. , 1962. The Impulse Response Function and Ship Motions. Schiffstechnik 47, 101–109.

Koo, W., Kim, M.H., 2004. Freely floating-body simulation by a 2D fully nonlinear numerical wave tank. Ocean Engineering 31, 2011–2046.

Ma, G., Farahani, A.A., Kirby, J.T., Shi, F., 2016. Modeling wave-structure interactions by an immersed boundary method in a σ-coordinate model. Ocean Engineering 125, 238–247.

Orszaghova, J., Wolgamot, H., Draper, S., Rafiee, A., 2018a. Motion instabilities in tethered buoy wecs, in: Asian Wave and Tidal Energy Conference, Taipei, Taiwan.

Orszaghova, J., Wolgamot, H., Eatock Taylor, R., Taylor, P.H., Rafiee, A., 2018b. Transverse motion instability of a submerged moored buoy. Proceedings of the Royal Society A: Mathematical, Physical and Engineering Sciences

Paulling, J., Rosenberg, R., 1959. On unstable ship motions resulting from nonlinear coupling. Journal of Ship Research 3, 36–46.

Rijnsdorp, D.P., Hansen, J.E., Lowe, R.J., 2018. Simulating the wave-induced response of a submerged wave-energy converter using a non-hydrostatic wave-flow model. Coastal Engineering 140, 189–204.

Rijnsdorp, D.P., Zijlema, M., 2016. Simulating waves and their interactions with a restrained ship using a non-hydrostatic wave-flow model. Coastal Engineering 114, 119–136.

Stelling, G., Zijlema, M., 2003. An accurate and efficient finite-difference algorithm for non-hydrostatic free-surface flow with application to wave propagation. International Journal for Numerical Methods in Fluids 43, 1–23.

Zijlema, M., Stelling, G., Smit, P., 2011. SWASH: An operational public domain code for simulating wave fields and rapidly varied flows in coastal waters. Coastal Engineering 58, 992–1012.